The effect of Zr(IV) addition on the phosphate removal properties of MgAl-LDH

Kamilla Thingholm Bünning, Tae-Hyun Kim, Vanessa Prevot, Claude Forano, Ulla Gro Nielsen

The effect of Zr(IV) addition on the phosphate removal properties of MgAl-LDH

Kamilla Thingholm Bünning[a], *Tae-Hyun Kim*[a,b], *Vanessa Prevot*[c], *Claude Forano*[c], *Ulla Gro Nielsen*[*,a]

[a]Department of Physics, Chemistry, and Pharmacy, University of Southern Denmark, 5230 Odense M, Denmark

[b]Laboratory of Accelerator and Radioisotopes, Korea Atomic Energy Research Institute, Jeongeup 56212, Korea

[c]Université Clermont Auvergne, CNRS, ICCF, F-63000 Clermont-Ferrand, France

*E-mail: ugn@sdu.dk. Phone: +45 6550 4401

Abstract

Recovery of phosphate from wastewater represents a sustainable alternative to phosphate rock, a limited resource. Magnesium aluminum layered double hydroxides (MgAl-LDH), are promising sorbents due to their high phosphate removal capacity by ion-exchange (26-124 mgP/g). Furthermore, an increased sorption capacity has been reported by the addition of zirconium (Zr(IV)) into the LDH lattice. However, ambiguity exists especially in relation to the incorporation of Zr and the stability of the MgAl-LDH. To understand how Zr(IV)-addition affects the phosphate sorption properties (both capacity and mechanism) on the atomic level, solid state multi-nuclear NMR spectroscopy was combined with complimentary characterization techniques to study a series of MgAl-LDH with Zr to Al ratios of 1:9 and 1:1, which had the Mg to (Al+Zr) ratio fixed at 2:1. The LDH were synthesized by coprecipitation and subsequently aged or hydrothermally treated to improve the crystallinity (particle size). No evidence of Zr(IV) incorporation in the LDH was observed, instead Zr was present as Zr(IV)-hydroxide (X-ray amorphous) and crystalline Zr(IV) oxide after aging and hydrothermal treatment, respectively. The segregation of Zr(IV)and resulting lower Al content in the MgAl-LDH decreased the phosphate sorption capacity from 45-54 to 16-20 mgP/g. Zr (hydr)oxide impurities contributed with less than 5 mgP/g. Moreover, ^{31}P MAS NMR spectroscopy quantified showed that the MgAl-LDH contribute to less than 60% of the total P removal capacity.

Keywords: Layered double hydroxides; phosphate; sorption; environmental remediation; solid state NMR spectroscopy

1. Introduction

The global phosphorous (P) challenge receives increasing attention since phosphorous in the form of orthophosphate ($H_xPO_4^{(3-x)-}$), is a fertilizer vital for global food security (Cordell et al., 2009; Cordell and White, 2014; Jupp et al., 2021; Reitzel et al., 2019). Traditionally, phosphate has been extracted from phosphate rock (Cordell et al., 2009; Jupp et al., 2021), a non-renewable resource, and depletion is in the worst-case predicted within the next century (Jupp et al., 2021; Walan et al., 2014). A promising alternative is the recovery of phosphate accumulated in municipal and industrial wastewater at wastewater treatment plants (Bunce et al., 2018; Egle et al., 2016). Current recovery approaches include the use of sludge and struvite ($NH_4MgPO_4 \cdot 6H_2O$) as a fertilizer, whereas vivianite ($Fe_3(PO_4)_2 \cdot 8H_2O$) is an emerging technology (Hall et al., 2020; Lamastra et al., 2018; Rahman et al., 2014; Talboys et al., 2016; Wilfert et al., 2015). The use of selective and ideally reusable phosphate (ad)sorbents is a promising, but less developed technology (Wu et al., 2020). Layered double hydroxides (LDH) have great potential due to a high affinity for orthophosphate and ion-exchange capacity (26 - 124 mgP/g), depending on, e.g., the phosphate speciation ($H_2PO_4^-$, HPO_4^{2-}, PO_4^{3-}) and LDH composition (Table S1) (Ashekuzzaman and Jiang, 2014; Luengo et al., 2017; Lundehøj et al., 2019a; Lundehøj et al., 2019b; Novillo et al., 2014). Phosphate can subsequently be recovered and the LDH reused or the phosphate loaded LDH can directly be applied as a fertilizer (Bernardo et al., 2018; Borges et al., 2019; Everaert et al., 2016).

LDH have the general formula $[M(II)_{1-x}M(III)_x(OH)_2]^{x+}(A_{x/n}^{n-}) \cdot yH_2O$ (x typically 0.2 - 0.33), whereas M(II) and M(III) are divalent and trivalent cations and A^{n-} is a charge compensating anion located in the interlayer together with water (Duan and Evans, 2005; Forano et al., 2006; Pushparaj et al., 2015). Subsequently, the LDH will be abbreviated as M(II)M(III)-LDH. Especially, the charge density (x), intercalated anion (A^{n-}), particle size, pH, and competing anions are important parameters related to the removal capacity and stability of the LDH.

For environmental applications, mainly the non-toxic MgFe -, CaAl -, CaFe -, and MgAl-LDH are relevant (Al Jaberi et al., 2019; Ashekuzzaman and Jiang, 2014; Bekele et al., 2019; Kim et al., 2020; Luengo et al., 2017; Lundehøj et al., 2019b; Novillo et al., 2014). MgAl-LDH is the most promising for phosphate removal, since the other LDH are highly unstable upon phosphate exposure (Al Jaberi et al., 2019; Bekele et al., 2019; Kim et al., 2020).

To enhance the function of LDH such as the phosphate sorption capacity, modification of LDH with high-valent cations, especially Zr(IV) has been proposed. The rationale is that the Zr(IV) will increased the cation layer charge and thereby the anion exchange capacity as Zr(IV) is speculated to replace Al(III)(Arias et al., 2018; Chitrakar et al., 2010; He et al., 2021; Koilraj and Kannan, 2010; Liu et al., 2014; Miyauchi et al., 2009; Nowicki et al., 2016; Poonoosamy et al., 2018; Velu et al., 1998; Wang et al., 2018; Wang et al., 2017). For example, incorporation of a Zr(IV) instead of a Al(III) in the brucite layer would require one HPO_4^{2-} instead of half a HPO_4^{2-} for charge balance. This leads to a higher anion-exchange capacity.

An increased P removal capacity has also been reported for Zr(IV) modified LDH as compared to the corresponding M(II)M(III)-LDH in phosphate solution, seawater, and wastewater (Table 1). However, most studies compare the P removal capacity of the Zr-modified LDH with the parent LDH, which has carbonate as interlayer anion, c.f., Table 1. This suppresses the phosphate removal by the anion-exchange pathway, due to the high affinity of the LDH for carbonate (Forano et al., 2006; Lundehøj et al., 2019b; Nuryadin et al., 2021). Therefore, the increased phosphate removal capacity obtained by addition of Zr can instead be explained by the co-presence of impurities such as Zr(IV) (hydr)oxides, which also have a significant phosphate removal capacity (Table 1).

Table 1. Phosphate removal capacities (mgP/g) determined for Zr-doped LDH and the corresponding parent M(II)M(III)-LDH reported in literature and the current work. The chemical composition (M(II), M(III), anion) of the LDH, which was prepared by co-precipitation, the post synthesis treatment employed (aged or hydrothermal treated, HT), and the water medium tested (seawater, wastewater, phosphate solution) and the phosphate concentration(s) used (mgP/L). The P removal capacity for $Zr(OH)_4$ and ZrO_2 are given for a comparison. Finally, whether the conclusion was successful Zr doping into the LDH or not (yes/ no). RT = room temperature. HT = hydrothermal treatment. * = two phase system (M(II)M(III)-LDH and Zr-phase) purposely prepared.

Cations	Treatment	Anion	Solution (mgP/ L)	M(II)/(M(III)+Zr)	M(III):Zr	P removal (mgP/ g)	Zr in LDH layer?	References
Mg, Al	Aged (RT)	CO_3^{2-}	P enriched seawater (0 - 0.33)	3	1	25	Yes	(Chitrakar et al., 2007)
	Aged (RT)	Cl^-		3	1	9	Yes	
	Aged (RT)	CO_3^{2-}		Not available	NA	1	NA	
	Aged (RT)	CO_3^{2-}	Phosphate (1 - 10)	3	1	39	Yes	
	Aged (RT)	Cl^-		3	1	22	Yes	
	Aged (RT)	CO_3^{2-}	Phosphate (100)	3	1	50	Yes	
	Aged (RT)	Cl^-		3	1	30	Yes	
Zn, Al	Aged (65°C)	CO_3^{2-}	Phosphate (10 - 250)	2 - 4	2.5	25 - 91	Yes	(Koilraj and Kannan, 2010)
	Aged (65°C)	CO_3^{2-}		2 - 4	NA	9 - 60	NA	
Mg, Al	Aged (RT)	CO_3^{2-}	P enriched seawater (0.33)	4	1	18	No	(Miyauchi et al., 2009)
	Aged (RT)	CO_3^{2-}		4	NA	1.3	NA	
	HT (120°C)	CO_3^{2-}		4	1	10	No	
	HT (120°C)	CO_3^{2-}		4	NA	0.6	NA	
Mg, Fe	Aged (RT)	CO_3^{2-}	P enriched seawater (1 - 30)	2 - 4	1	15 - 27	No	(Chitrakar et al., 2010)
	Aged (RT)	Cl^-		Not available	NA	≈ 3	NA	
	Aged (RT)	CO_3^{2-}	Phosphate (100)	2 - 4	1	20 - 35	No	
	Aged (RT)	Cl^-		Not available	NA	≈ 50	NA	
Mg, Fe	Aged (80°C)	CO_3^{2-}	Phosphate (1 - 50)	Not available	2 - 0.5	35	No *	(Nuryadin et al., 2021)
	Aged (80°C)	CO_3^{2-}		Not available	NA	18	NA	
Mg, Al	Aging (RT)	CO_3^{2-}	Phosphate (5 - 200)	Not available	NA	70	NA	(Motandi et al., 2022)
	Aging (RT)	CO_3^{2-}		Not available	Not available	99	No *	
ZrO_2	Not available	None	Seawater (0.33)	Not available	Not available	1 - 12	Not available	(Miyauchi et al., 2009)
$Zr(OH)_4$	Not available	None	Synthetic wastewater (10)	Not available	Not available	19 - 30	Not available	(Johir et al., 2016)
$Zr(OH)_4$	Not available	None	Phosphate (7 - 114)	Not available	Not available	38	Not available	(Luo et al., 2017)
Mg, Al	HT (120°C)	Cl^-	Phosphate (18 - 224)	2	No Zr	45(2)	No Zr	This work
	Aging (80°C)	Cl^-		2	No Zr	54(2)	No Zr	
	HT (120°C)	Cl^-	Phosphate (18 - 224)	2	9	43(2)	No	This work
	Aged (80°C)	Cl^-		2	9	47(2)	No	
	HT (120°C)	Cl^-	Phosphate (18 - 224)	2	1	16(2)	No	This work
	Aged (80°C)	Cl^-		2	1	20(2)	No	

NA, not applicable as Zr was not used during the synthesis.

92

Studies have also investigated the physical mixtures of MgAl-LDH and Zr-(hydr)oxide with the goal to either prepare nano-sized particle (ad)sorbents as Zr-(hydr)oxide on the surface of LDH can suppress crystal growth (Nuryadin et al., 2021) or to modify the layer charge by the introduction of Zr(IV)-O^{2-} acid base pairs (Motandi et al., 2022). Here an increased P removal capacity for a mixed system was also reported (Table 1).

Several studies have concluded a successful incorporation of Zr(IV) into the LDH. However, the successful incorporation of Zr(IV) into the LDH structure was mainly based on the analysis of low-quality powder X-ray diffractograms and/ or the qualitative variation of the M-M distance derived from the (110) reflection (Velu et al., 1998; Wang et al., 2018). Thus, the insertion of Zr(IV) was, in part, concluded based on an expansion of the unit cell parameter *a* with increasing Zr(IV) content in ternary M(II)AlZr-LDH (Chitrakar et al., 2007; Koilraj and Kannan, 2010; Shen et al., 2011; Velu et al., 1998; Wang et al., 2018). A slight reduction in interlayer spacing (7.9 to 7.8 Å) based on visual inspection of PXRD data was ascribed to an increased charge of the cation layer for NiAl-LDH with nitrate as interlayer ion, i.e. successful incorporation of Zr(IV) into the LDH (Wang et al., 2017). However, for LDH with nitrate as interlayer ion, a lower Al^{3+} results in a decreased interlayer spacing, as nitrate ion can be parallel to the cation layer (Karthikeyan et al., 2021). However, a reduced Al content in a $M(II)_{1-x}Al_x$-LDH will give a similar structural trend. Thus, it is not possible to distinguish between *i)* the incorporation of Zr(IV) into the LDH and *ii)* the formation of both MgAl-LDH and a Zr (hydr)oxide phase only by PXRD and bulk chemical analyses.

In more rigorous studies, the use of advanced structural characterization techniques and in depth data analyses have clearly shown, that Zr(IV) was not incorporated into the LDH, but instead a mixture of LDH and $Zr(OH)_4$ (or ZrO_2) was obtained (Intissar et al., 2003; Miyauchi et al., 2009). For example (Intissar et al., 2003) investigated the local environment of metal cations for a series of

$M(II)_{0.75}Al_{0.25-y}M(IV)_y(OH)_2(CO_3)_{(y+0.25)/2},nH_2O$ (M(II) = Mg, Co; M(IV) = Sn, Zr) LDH using X-ray absorption spectroscopy (XAS) and Mössbauer spectroscopy combined with detailed data analysis. This clearly confirmed that the first metal ion coordination sphere for both Zr(IV) and Sn(IV) was dominated by M(IV)-M(IV) correlations, i.e., the formation of separate Sn(IV) and Zr(IV) phases. Similarly, (Miyauchi et al., 2009) showed that ZrMgAl-LDH synthesized by coprecipitation had the same k^3-weighted Zr-K edge as ZrO_2 in the extended X-ray absorption fine structure (EXAFS) spectra. Additionally, zirconium oxide impurities are generally only observed after hydrothermal treatment above approximately 120°C (Chitrakar et al., 2007), an approach usually employed to increases the LDH particle size and thereby stability (Pushparaj et al., 2015). Such impurities were not observed, when the LDH was aged below 100°C, a more common post synthesis treatment (Table 1). However, amorphous Zr phases such as $Zr(OH)_4$ or ZrO_2 may still be present and not observed by Powder X-ray Diffraction (PXRD), the routine characterization method.

A suite of bulk and atomic level characterization methods is necessary to link the phosphate removal capacity and pathways to the LDH properties (chemical composition, particle size, etc.). For example, inductively coupled plasma (ICP) spectroscopy and PXRD provides information about the bulk content and crystalline phases, respectively, whereas solid state NMR spectroscopy (SSNMR) gives detailed insight into the atomic level structure of the LDH and (amorphous) impurities and/ or other phases (Nielsen, 2021). SSNMR combined with PXRD, electron microscopy, and elemental analysis is crucial to obtain detailed insight into the LDH composition and anion-exchange properties (Kim et al., 2020; Lundehøj et al., 2019a; Pushparaj et al., 2015).

In contrast to previous studies, we have performed a detailed investigation on how Zr(IV) addition affects the phosphate removal capacity and pathways for MgAl-LDH with chloride (Cl^-) as the

interlayer anion prepared by two common post-synthesis treatments (aging and hydrothermal treatment). This provided detailed insight into the different phosphate removal pathways and their relative contributions. Thus, our goal was to assess if Zr(IV) addition will improve the performance of MgAl-LDH based sorbents with a view to reusability. This was obtained by combining conventional phosphate sorption isotherm and kinetics experiments with characterization of the LDH before and after phosphate exposure using PXRD, FT-IR, inductively coupled plasma - optical emission spectrometry (ICP-OES), zeta (ζ) potential measurements, electron microscopy (SEM, TEM), and multinuclear MAS NMR spectroscopy.

2. Experimental section

2.1. Materials

$MgCl_2 \cdot 6H_2O$ (≥98% purity), $AlCl_3 \cdot 6H_2O$ (≥99% purity), $ZrO(NO_3)_2 \cdot xH_2O$ (≥99% purity), NaOH (≥97% purity), NaCl (≥99% purity) and K_2HPO_4 (≥ 98% purity), purchased from Sigma-Aldrich, and HCl (≥37%) purchased from Fisher Scientific, were used for the synthesis and sorption experiments without further purification.

2.2. Methods

2.2.1. Sample preparation

The metal- and alkaline salts were dissolved in decarbonated water prepared by boiling milli-Q water with nitrogen (N_2) flow for ca. one hour and then cooled to 25-35 °C under a nitrogen (N_2) flow before use. MgAl- and Zr doped MgAl-LDH were synthesized by coprecipitation at constant pH using earlier reported procedures (Chitrakar et al., 2007) with the following modifications: 500 mL of a metal ion solution containing Mg^{2+} , Al^{3+}, and Zr^{4+} with a total metal ion concentration of 0.6 M

and 500 mL of an alkaline solution containing 1.2 M NaOH and 0.6 M NaCl were prepared. For each sample, the individual metal ion concentrations and mole percent are given in Table 2. 400 mL of the metal solution was added at a rate of 1.33 mL/min using a titrator (905 Titrando®; Metrohm AG, Herisau, Switzerland) into a 1 L three-necked-round-bottom flask which already contained 100 mL of decarbonated water under magnetic stirring (600 - 800 rpm). Simultaneously, the alkaline solution was added to maintain the pH at 10.0(2) at a rate like that for the metal solution. All synthesis were performed under a N_2 flow to minimize carbonate impurities.

Table 2. The absolute concentrations of the metal cation solutions (mol/L) used in the syntheses with the relative percentage of Mg, Al and Zr (mol%) in the parenthesis. Moreover, the metal ion composition (mol%) for Mg, Al, and Zr for the synthesized LDH and these LDH after phosphate exposure. n. a. = not applicable.

Sample	**Synthesis conditions (mol/L) / (mol%)**			**Synthesized composition (mol%)**			**Composition after P exposure (mol%)**		
	Mg	Al	Zr	Mg	Al	Zr	Mg	Al	Zr
MgAl-A	0.4 (66.7)	0.2 (33.3)	0 (0)	66.3(2)	33.7(1)	n. a.	65.5(1)	34.5(1)	n. a.
MgAl-HT	0.4 (66.7)	0.2 (33.3)	0 (0)	66.0(1)	34.0(1)	n. a.	65.7(3)	35.2(1)	n. a.
Zr0.1-A	0.4 (66.7)	0.18 (30.0)	0.02 (0.03)	66.7(1)	30.9(1)	2.3(1)	67.0(2)	31.9(1)	1.1(1)
Zr0.1-HT	0.4 (66.7)	0.18 (30.0)	0.02 (0.03)	68.6(1)	28.8(1)	2.5(1)	66.9(1)	31.8(1)	1.3(1)
Zr0.5-A	0.4 (66.7)	0.1 (16.7)	0.1 (16.7)	70.1(1)	18.6(1)	11.3(1)	68.3(1)	19.4(1)	12.3(2)
Zr0.5-HT	0.4 (66.7)	0.1 (16.7)	0.1 (16.7)	74.8(1)	19.7(1)	5.5(1)	72.6(1)	20.6(1)	6.8(1)
$Zr(OH)_4$	0 (0)	0 (0)	0.2 (100)	n. a.	n. a.	n. a.	n. a.	n. a.	n. a.
ZrO_2	0 (0)	0 (0)	0.2 (100)	n. a.	n. a.	n. a.	n. a.	n. a.	n. a.

After addition of the metal- and alkaline solutions, the obtained solids were isolated by centrifugation (10.000 rpm, 10 min) using a Sigma Laboratory Centrifuge (2-16P) and then roughly divided into two batches: the first batch was redispersed into 350 mL of decarbonated water and aged at 80°C in a 500 mL three-necked-round-bottom flask under reflux and magnetic stirring for 16 h. The

second batch was redispersed into decarbonated water (350 mL) and subsequently hydrothermally treated in multiple 70 mL Teflon® lined steel autoclaves (ca. 2/3 filled) for 16 h at 150°C in a Binder GmbH oven. Subsequently, both batches, were washed with 40 mL deionized water in 50 mL conical centrifuge tubes (Sarstedt, 114×28 mm) and shaken thoroughly followed by removal of the supernatant after centrifugation (10.000 rpm, 10 min). The washing was repeated thrice. Finally, zirconium hydroxide ($Zr(OH)_4$) and zirconium oxide (ZrO_2) were synthesized using 500 mL of a 0.2 M $ZrO(NO_3)_2 \cdot xH_2O$ and 500 mL of 1.2 M NaOH solution using the same titrator, volume, metal-solution rate, and pH as above. After synthesis, the batch was also divided into two and the post-synthesis was either aging or hydrothermal treatment. Aging resulted in the formation of amorphous $Zr(OH)_4$, whereas crystalline ZrO_2 was obtained after hydrothermal treatment. All solid products were dried at 50°C overnight (≈ 16-18 h) and ground to a fine powder using an agate mortar and pestle before analyses.

Table 2 summarized the nomenclature for all materials and their synthetic compositions. Briefly, MgAl-A and MgAl-HT corresponds to conventional MgAl-LDH with either aging (A) at 80°C or hydrothermally treatment (150°C, HT), respectively. The Zr modified LDH are named after their ideal composition based on the reactant ratioss: Zr0.1-A and Zr0.1-HT corresponds to the LDH synthesized with Zr^{4+} and Al^{3+} concentration of 0.02 mol/L and 0.18 mol/L, respectively. This corresponds to an Al to Zr ratio of 9 to 1; Al/Zr = 9/1), and ideally a $Mg_2Al_{0.9}Zr_{0.1}$-LDH, whereas Zr0.5-A and Zr0.5-HT are MgAl-LDH synthesized with 0.1 mol/L Zr^{4+} and 0.1 Al^{3+} (Al/Zr = 1/1, ideally $Mg_2Al_{0.5}Zr_{0.5}$-LDH). Al/Zr = 1 was chosen to match earlier studies (Table 1) whereas the ratio Al/Zr = 9 were selected to investigate if a small Zr(IV) doping was masked by the Zr(IV) impurities in the Al/Zr = 1 samples. For samples obtained after P exposure a ”-P” is added as a suffix, for example MgAl-HT-P is MgAl-HT after phosphate exposure.

2.2.2. *Phosphate isotherm batch experiments*

The phosphate sorption isotherm experiments were performed in 15 mL polypropylene conical centrifuge tubes (Sarstedt, 120×17 mm) containing 10.00 mL phosphate solution and 10.0(1) mg LDH, which were shaken at 400 rpm using an orbital shaker for 24 h at room temperature (≈ 20°C). All phosphate isotherm experiments were performed as duplicates. The concentration of the phosphate solutions ranged from 30 to 400% (≈ 18 to 224 mgP/L) theoretical anion exchange capacity (TAC) for HPO_4^{2-} calculated for a $Mg_2Al(OH)_6Cl{\cdot}2H_2O$ LDH under the assumption of the complete ion exchange of Cl^- for HPO_4^{2-} (Table S1). The pH of the solutions was adjusted to 7.5 (67% HPO_4^{2-}, 33% $H_2PO_4^-$) using 0.1 M HCl. To mimic industrial applications of LDH sorbents, the pH was not actively controlled. Moreover, pH control is known to drive the dissolution of the LDH with the lowest dissolution observed at pH 8 (Imran et al., 2016). After 24 h, the supernatant was collected using a 2 mL disposable pipette and filtrated through a 0.45 µm PTFE syringe filter. All phosphate solutions were prepared in milli-Q water.

The ortho-phosphate concentration was quantified by the molybdate blue method (Nagul et al., 2015) using a UV-Vis-spectrometer (UV-600PC; VWR, U.S.A) at 880 nm. The equilibrium phosphate sorption (q_e (mgP/g)) capacity were then calculated using *Eq. 1* and plotted as a function of the equilibrium concentration (C_e (mgP/L)), i.e., the concentration in the solution remaining at the end of the experiment. Lastly, the sorption isotherms were modelled by the Langmuir (*Eq. 2*) and Freundlich (*Eq. 3*) models using Origin (Version 2017, OriginLab Corporation).

$$q_e = (C_o - C_e)\cdot(V / m) \qquad (Eq.\ 1)$$

$$q_e = (Q_m K_L C_e)/(1 + K_L C_e) \qquad (Eq.\ 2)$$

$$q_e = K_F C_e^{1/n} \qquad (Eq.\ 3)$$

Where C_0 is the initial concentration (mgP/L), V (L) is the total volume and m (g) is the mass of LDH. Q_m is the maximum monolayer coverage (mgP/g), K_L is the Langmuir isotherm constant (ml^3/mg) related to the affinity of binding sites, K_F (mgP/g) is the Freundlich constant (related to the sorption capacity) and n is related to the sorption intensity (Foo and Hameed, 2010).

2.2.3. Powder X-ray diffraction

PXRD were recorded on a Rigaku Miniflex 600 X-ray diffractometer using Cu Kα radiation (λ = 1.5406 Å) with Kβ-filter and a D/Tex Ultra-high-speed silicon strip detector using a voltage of 40 kV and a current of 15 mA from 2θ = 5 to 70°, with a step size of 0.02° at 10 degrees per minute. Le Bail fitting was performed to determine the cell-parameters using the FullProf software (Rodríguez-Carvajal, 1993). The structural model used a Zn_2Al-Cl LDH (ICSD code 155051) as starting structures (where Zn were exchanged for Mg) (ICSD code 155051) (Lombardo et al., 2005). For Zr0.5-HT the CIF for ZrO_2 (ICSD code 105553 (Katz, 2006) was also used in the refinement. Both CIF were found through search-and-match in the PXRD software PDXL2. Generally, the parameters refined were W, X, U, cell parameters (a and c), shape1, B_{ov}, zero shift, and the background. The background was chosen manually by linear interpolation and described by the Pseudo-Voigt function. A Le Bail refinement was chosen instead of Rietveld refinement due the complexity of the reflection in mid angles (2θ ≈ 30 - 50°), resulting from stacking faults and/ or mix of multiple polytypes. Next, the average crystallite size was estimated using the Scherrer equation (Eq. 4) for the (003) reflection and experimental broadening was corrected for using the (111) reflection at 2θ = 28.5° (FWHM = 0.10°) for a Si standard. The full-width-half-max (FWHM) used for calculation of crystallite size were likewise calculated in WinPLOTR in FullProf suite.

$$B(2\theta_{003}) = (K \cdot \lambda)/(\tau \cdot \cos(\theta)) \qquad (Eq.\ 4)$$

Were $B(2\theta)$ is the FWHM of the (003) peak, K is the crystallite shape constant (here approximated to 0.9 assuming a spherical morphology (Forano et al., 2006), λ is the wavelength, θ is the diffraction angle, and τ is the crystallite diameter in Ångstrøm (Å).

2.2.4. Solid State ^{1}H, ^{27}Al, and ^{31}P MAS NMR spectroscopy

Single pulse ^{27}Al and ^{31}P magic angle spinning (MAS) NMR spectra and ^{27}Al triple quantum magic angle spinning (3QMAS) NMR spectra were recorded on a JEOL ECZ500CR 500 MHz NMR spectrometer (11.7 T) using a 3.2 mm double resonance MAS NMR probe with 15 kHz spinning speed for the single pulse and 14 - 15 kHz for the 3QMAS experiments. The relaxation delay was optimized for each sample but were generally 1 s for the single pulse ^{27}Al MAS NMR (< 10° pulse width for quantitative excitation) and 30 - 90 s for single pulse ^{31}P MAS NMR (45° excitation pulse). The ^{27}Al 3QMAS experiment were recorded using a three-pulse z-filter sequence (Amoureux and Fernandez, 1998).

Single pulse ^{1}H MAS NMR spectra were recorded on an Agilent Inova 600 MHz NMR spectrometer (14.1 T) using a 1.6 mm triple resonance MAS NMR probe and 30 - 32 kHz spinning speed. The ^{1}H, ^{27}Al, and ^{31}P and NMR spectra were referenced using H_2O ($\delta_{iso}(^{1}H)$ = 4.6 ppm), 1.0 M solution of $AlCl_3$ ($\delta_{iso}(^{27}Al)$ = 0 ppm) and concentrated phosphoric acid (85% H_3PO_4; $\delta_{iso}(^{31}P)$ = 0 ppm), respectively. Deconvolution of the ^{27}Al single pulse MAS NMR spectra were performed in Quadfit (Kemp and Smith, 2009) using two sites: one with C_Q = 1.6 MHz and η = 0 (LDH) and a second site with C_Q = 3.3 MHz and η = 0.2 (amorphous aluminum hydroxide, will be discussed later) (Jensen et al., 2016; Pushparaj et al., 2015; Staal et al., 2017). The ^{27}Al 3QMAS NMR spectra were

processed in ssNake (v1.1), (van Meerten et al., 2019) whereas single-pulse ^{1}H and ^{31}P MAS NMR spectra were analyzed by deconvolution in MestReNova (ver. 14.2.1.).

2.2.5. Zeta potential - and hydrodynamic size measurements

The zeta (ζ) potential of MgAl/Zr composite, $Zr(OH)_4$, and ZrO_2 were determined by electrophoretic light scattering utilizing a Zetasizer nano ZS analyzer from Malvern Panalytical fitted with a 4 mW 632.8 nm "red" laser. For the measurement, powdered samples were dispersed (ca. 0.1 mg/mL) in deionized water and stirred 24 h and then sonicated for 15 min at room temperature. The Zeta potential values were calculated by determining the electrophoretic mobility and then applying the Henry equation.

2.2.6. Transmissions electron microscopy

Transmission electron microscopy (TEM) images were acquired with a JEOL 2100Plus microscope (200 kV) fitted with LaB_6 electron gun. Elemental analysis of individual particles was acquired by energy dispersive X-ray spectroscopy. 20 µL of an aqueous suspension of 1 mg sample per mL water was deposited on a carbon grid covered with a forward carbon film and dried at 40°C under air.

2.2.7. Elemental analysis

Inductively coupled plasma optical emission spectrometry (ICP-OES) was used for the quantification of Mg, Al, Zr, and P.. Approximately 0.02 g LDH and 10.00 mL of concentrated nitric acid (HNO_3, 65%) were mixed followed by microwave digestion at 200°C for 15 min. The resulting

supernatant were diluted appropriately in milli-Q water beforeanalysis on an Optima 2100 DV, PerkinElmer, USA.

3. Results and discussion

3.1. The effect of the Zr content on the phosphate removal capacity of MgAl-LDH

The successful synthesis of hydrotalcite LDH was confirmed for all samples based on the observation of the characteristic (003), (006), and (110) reflections by PXRD (Figure 1). However, the phosphate sorption capacity of the LDH samples will be presented prior to detailed analysis of the PXRD data. Sorption will in the following be used to describe the phosphate removal properties of the LDH materials since multiple processes contribute including surface sorption, ion-exchange, and the removal of P by impurity phases. The individual contribution cannot be distinguished unambiguously from the sorption data alone.

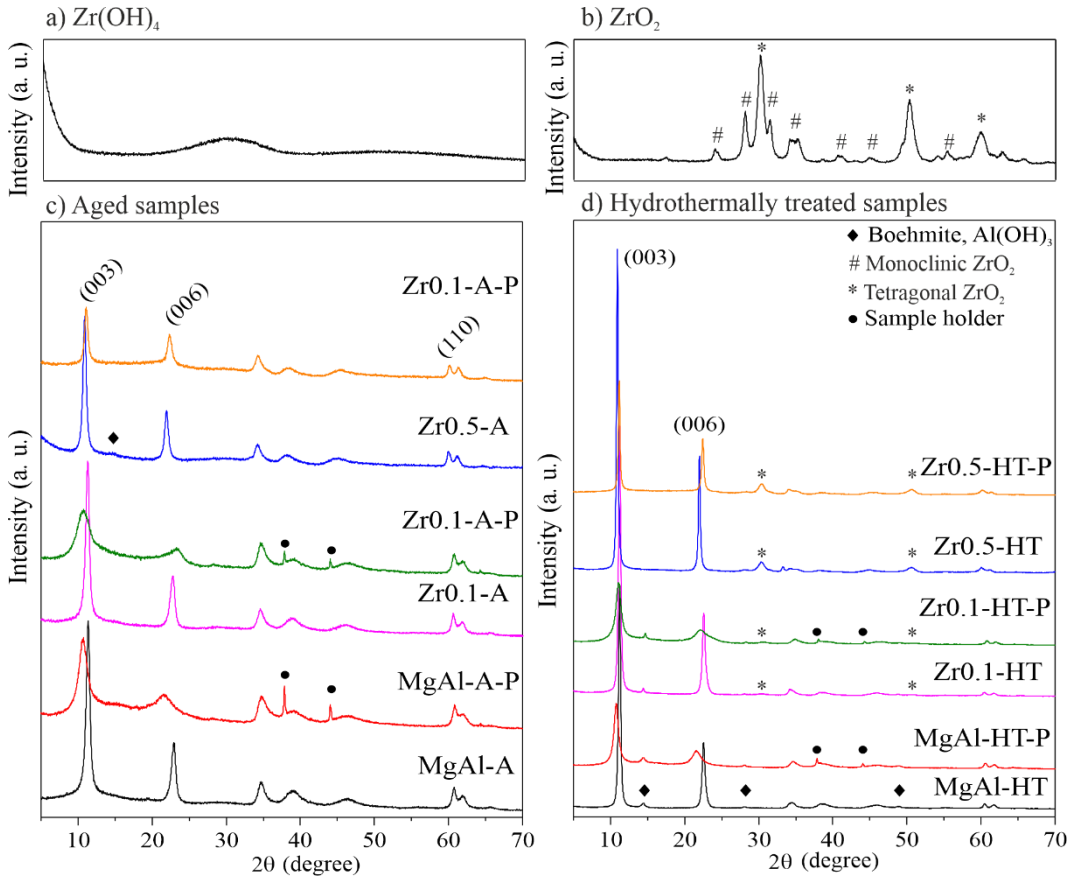

Figure 1. PXRD diffractograms of the synthesized LDH samples and these after phosphate exposure for c) aged samples and d) hydrothermally treated samples, as well as of $Zr(OH)_4$ (a) and ZrO_2 (b). The reflections from the sample holder (•) are observed in some diffractograms due to limited sample quantities.

The phosphate removal capacity as a function of both the time and the concentration were obtained from sorption kinetics and isotherms. The sorption isotherm does not reach a clear plateau, even at 400% TAC (Figure 2). Visual inspection of the isotherm shows that two sequential processes contribute (Figure 2). First, one process at low equilibrium concentrations, below a C_e of approximately 75 mgP/L, and a second above. This is explained by the presence of multiple phosphate removal mechanisms: both ion-exchange, adsorption to the LDH surface (e.g., charge interactions, grafting),

and adsorption to impurities (details in the next section) may result in phosphate removal. Moreover, dissolution of the LDH and/or Zr(IV) (hydr)oxides followed by precipitation of phosphate phases (e.g., Al-P, Mg-P) may also contribute. The contribution from two or more pathways explains the inadequately fitting by both the Freundlich (R^2 = 0.78 to 0.90) and Langmuir (R^2 = 0.56 to 0.91) (Figure S2, Table S2). Thus, the sorption capacity is estimated visually (Table 1) at the clear break-off in the isotherm due to these non-ideal fits, which is at about C_e of. Noteworthy, the kinetic sorption experiments showed a quick phosphate uptake and reached an equilibrium within the first hour (Figure S1).

In contrast to previous studies (Table 1), an increased Zr(IV) content in the LDH samples is accompanied by a drastic decrease in the phosphate adsorption capacity: For Zr0.5-A and Zr0.5-HT the experimental sorption capacity is only 20(2) and 16(2) mgP/g, respectively. The MgAl-A and MgAl-HT (conventional MgAl-LDH) exhibit the highest phosphate removal capacities of 54(2) and 45(2) mgP/g, respectively (see also Table 1). To understand this trend, detailed characterization of the samples was performed.

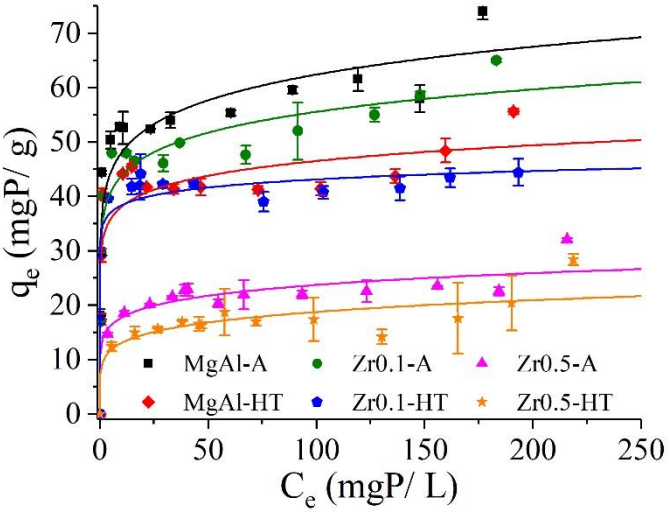

Figure 2. Phosphate sorption isotherm, which is inadequately modelled by both the Freundlich (shown) and Langmuir isotherms (Figure S2) with the parameters given in Table S2. Multiple processes contribute to the sorption capacity which was estimated visually at the break-off point (Table 1, see text). The error-bars are based on a duplicate of sorption experiments with triplicate determination of the phosphate concentration.

3.2.Characterization of the synthesized LDH with and without Zr doping

The parent LDH with and without Zr were characterized using PXRD, ICP-OES, FT-IR, TEM, SEM, ^{1}H, ^{25}Mg and ^{27}Al MAS NMR, and zeta potential measurements. The unit cell parameters for the pristine LDH were obtained by Le Bail fitting (Tables 3 and S3, Figure S3). For the LDH after phosphate sorption experiments, these were estimated based on the (003) and (110) reflections due to the increased complexity of the PXRD diffractograms. Agreement factors generally show a good fit with χ^2 values of 2 - 8 and R- and R_f-factors of < 3% (Table S3). Aged samples are less crystallinity (i.e., lower intensity, increased FWHM; Table 3) as compared to the samples after hydrothermal treatment (Figure S1), an observation in agreement with earlier studies (Pushparaj et al., 2015)

Table 3. Properties of the synthesized samples and these after phosphate exposure based on PXRD, SSNMR spectroscopy, ICP-OES, and zeta potential measurements. For a comparison, the zeta potential for $Zr(OH)_4$ and ZrO_2 were -18(5) and -8(4) mV respectively.

[a] The cell parameters obtained from Le Bail fitting (Figure S3), [b] Cell parameters based on the position of the (003) and (110) reflections. FWHM is for the (003) reflection. n. a. = Data not available. τ = is the crystallite size approximated from the Scherrer equation using the (003) reflection.

	***a* (Å)**	***c* (Å)**	**FWHM (°)**	***τ* (Å)**	**AOH (%Al)**	**x (^{27}Al+ICP)**	**x (^{1}H)**	**Zeta (mV)**
MgAl-A[a]	3.048(2)	23.303(3)	0.641(2)	124	29.0(3)	0.27(2)	0.23(2)	29(5)
MgAl-HT[a]	3.060(2)	23.617(3)	0.3249(6)	246	22.6(3)	0.28(2)	0.26(2)	27(6)
Zr0.1-A[a]	3.078(2)	23.417(3)	0.647(2)	123	29(2)	0.25(2)	0.20(2)	28(5)
Zr0.1-HT[a]	3.076(2)	23.576(3)	0.341(6)	234	19(1)	0.25(2)	0.27(2)	25(6)
Zr0.5-A[a]	3.080(2)	24.245(3)	0.526(2)	152	20(2)	0.18(2)	0.22(2)	12(4)
Zr0.5-HT[a]	3.092(2)	24.211(3)	0.2415(4)	330	< 5	0.20(2)	0.18(2)	30(5)
MgAl-A-P[b]	3.043(3)	24.859(4)	1.593(7)	50	32.0(2)	0.26(2)	n. a.	-17(4)
MgAl-HT-P[b]	3.054(3)	24.650(4)	0.775(2)	103	23.1(5)	0.29(2)	n. a.	-17(4)
Zr0.1-A-P[b]	3.047(3)	24.947(4)	2.30(12)	35	27(1)	0.26(2)	n. a.	-19(4)
Zr0.1-HT-P[b]	3.043(3)	23.935(4)	0.943(3)	85	26.0(1)	0.26(2)	n. a.	-18(4)
Zr0.5-A-P[b]	3.075(3)	23.861(4)	0.526(2)	152	21.8(3)	0.18(2)	0.21(2)	-11(4)
Zr0.5-HT-P[b]	3.073(3)	23.750(4)	0.2484(9)	331	9.5(3)	0.20(2)	n. a.	-9(4)

The *a*-cell parameter (the M-M distance) increased ca. 0.03 Å at highest Zr(IV) doping (Table 3, Figures S4). Diffractograms of MgAl-A and the Zr modified samples after aging (Zr0.1-A, Zr0.5-A) only contain LDH reflections (beside $Al(OH)_3$ impurities). In contrast, hydrothermal

treatment leads to the formation of additional crystalline phases (Figures 1 and S3). For MgAl-HT only boehmite (AlO(OH)) is detected, which is formed by dehydroxylation of Al hydroxides during the hydrothermal treatment (Pushparaj et al., 2016). In contrast, two new reflections are observed at $2\theta \approx 32°$ and 51° for the Zr modified LDH (Zr0.1-HT, Zr0.5-HT), which are assigned to ZrO_2 formed by dehydroxylation of $Zr(OH)_4$. This is supported by the conversion of amorphous $Zr(OH)_4$ to crystalline ZrO_2, when hydrothermally treated similar to the LDH samples. To identify the presence of $Zr(OH)_4$ in the aged samples FT-IR, TGA, TEM, SEM, and SSNMR were performed.

FT-IR spectra (Figure S5) of the pristine LDH, both with and without Zr(IV), exhibit the typical LDH bands including hydroxides (3500 - 3600 cm^{-1}), interlayer water (1600 - 1650 cm^{-1}), and the metal oxides bands, MO_6, (696 - 717 cm^{-1}) and OMO bands (500 - 400 cm^{-1}); M = metal cation (Goh et al., 2008; Staal et al., 2017). Minor carbonate contamination is also observed at 1350-1380 cm^{-1} due the high affinity of LDH for carbonate (Forano et al., 2006; Goh et al., 2008). When the Zr(IV) content is increased from 0.1 to 0.5 the intensity of the AlO_6 stretching mode (850-950 cm^{-1}) decreased strongly for both the aged and hydrothermally treated LDH samples. This indicates depletion of Al in the LDH cation layer corresponding to the reduced reactant concentration (Table 2).

From the single pulse ^{27}Al MAS- (Figure 3, Figures S6-7) and 3QMAS NMR two resonances are identified: Al in the LDH ($\delta_{iso}(^{27}Al) \approx 10$ - 12 ppm) and Al in amorphous Al hydroxide (AOH) ($\delta_{iso}(^{27}Al) \approx 5$ - 10 ppm) (Lundehøj et al., 2019b; Staal et al., 2017). The concentration of AOH is higher in the aged samples (30%) compared to hydrothermally treated (20%) samples, in accordance with earlier studies (Pushparaj et al., 2015; Staal et al., 2017). The adjusted Mg:Al ratio in the LDH phase was calculated using ICP-OES and ^{27}Al NMR (or ^{1}H MAS NMR; Table S4). They allresults in Mg:Al ratios within the known stable range for LDH (0.2 - 0.33) (Forano et al., 2006), as summarized in Table 3.

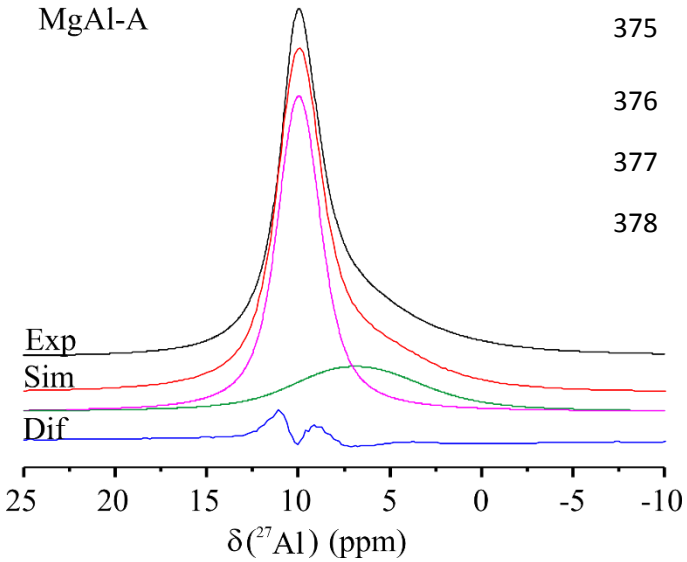

Figure 3. A representative deconvolution of a single pulse ^{27}Al MAS NMR spectrum using two phases: $\delta_{iso}(^{27}Al) \approx 10$ ppm (LDH, pink) and $\delta_{iso}(^{27}Al)$ centered at ≈ 7 ppm (AOH, green). The ^{27}Al MAS NMR spectra of the other samples, which are similar, are shown in Figures S6 and S7.

TGA (Figure S8) and ^{1}H MAS NMR (Figure 4, Figures S9-11) probed the thermal degradation and water content: Zr0.5-A exhibited a mass loss of 22(2)% and Zr0.5-HT of only 11(2)% below 200°C implying a higher water or hydroxide content in the aged sample compared to the hydrothermally treated. Moreover, ^{1}H MAS NMR showed an increased intensity around 5 ppm, which is ascribed to the overlap of the ^{1}H NMR resonances from $Zr(OH)_4$ ($\delta_{iso}(^{1}H) = 4.8$ ppm; Figure S9) and water in the LDH ($\delta_{iso}(^{1}H) = 4.5 - 5.0$ ppm; Table S4 and Figures S10-11). Deconvolution of the ^{1}H MAS NMR spectra showed resonances at $\delta_{iso}(^{1}H) \approx 4.8(2)$ ppm for Zr0.5-HT (26(5)%) and for Zr0.5-A (37(5)%) (Figure 4).

This intensity difference is ascribed to the presence of ^{1}H NMR resonance of $Zr(OH)_4$, which overlap with H_2O (see also Figure S9). Thus, $Zr(OH)_4$ must be present in Zr0.5-A. To further probe this, SEM provided insight into particle size, morphology, and homogeneity (Figure S12).

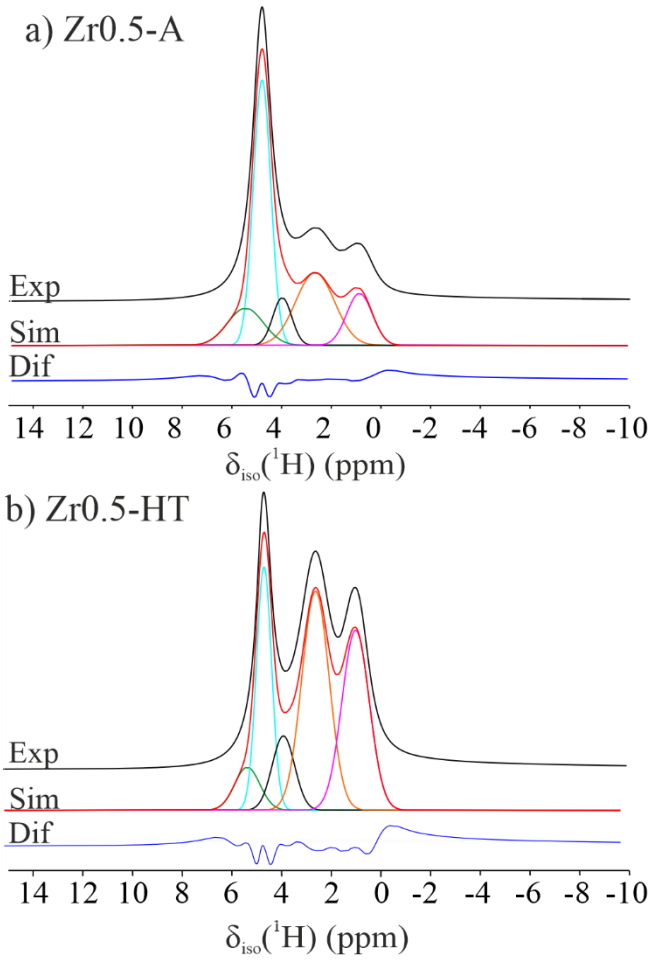

Figure 4. Deconvolution of the ^{1}H MAS NMR spectra of a) Zr0.5-A and b) Zr0.5-HT with the experimental (black), simulated (red), and difference between the experimental and simulated spectrum (dark blue), as well as the individual sites AOH (green), H_2O (turquoise), $Zr(OH)_4$, orange for Mg_2Al-OH, pink for Mg_3-OH and black is an unknown site needed for the satisfactory simulation of the experimental spectra.

401 Scanning electron microscopy (Figure S12) showed that MgAl-A and MgAl-HT consist
402 of hexagonal, plate-like particles with a width ranging from 200 to 600 nm, as typically observed for
403 LDH (Pushparaj et al., 2015). In addition, LDH with Zr added (Zr0.1-A, Zr0.5-A, Zr0.1-HT, Zr0.5-HT)
404 contain smaller ill-defined (< 100 nm) particles (see white arrows on Figure S12b, c, e, and f), which
405 are assigned to Zr phases (ZrO_2 and $Zr(OH)_4$ for Zr0.5-HT and Zr0.5-A respectively). Their presence is
406 also supported by TGA and ^{1}H MAS NMR.
407 Further characterization by transmission electron microscopy (TEM) of selected samples
408 (Figure 5), show that the hydrothermal treatment increases the particle size and improves the shape
409 homogeneity of the LDH-HT particles as compared to the particles aged at 80°C (Figure 5a and b).
410 Hydrothermal treatment prevents aggregation and favors a face-to-face orientation of individual
411 hexagonal platelets while for Zr0.1-A the particles are in dense,disordered agglomerates. EDX analysis
412 (Figure S13) reveal an increase in the Mg:Al ratio in the LDH from 2.0 to 2.5, for Zr0.1-A and Zr0.1-
413 HT respectively.. ZrO_2 nanoparticles (≈10 nm) are clearly observed on the surface of Zr0.1-HT
414 platelets as well as dispersed black spots (Figure 5B). The absence of these dark spots on the TEM
415 images of Zr0.1-A confirms the formation of amorphous $Zr(OH)_4$ nanoclusters most likely covering
416 the LDH surface as also observed by ^{1}H MAS NMR, TGA, and SEM analysis.
417 It is clear that the hydrothermal treatment converts these highly dispersed $Zr(OH)_4$
418 nanoclusters into ZrO_2 nanoparticles, which are very evident in the TEM images, as illustrated for
419 Zr0.5-A (Figure S14c and d). The sorption of phosphate on both the Zr0.1-A and Zr0.1-HT samples
420 forces the collapse of individual particles into densely packed aggregates most likely due to the change
421 in surface charge properties and inversion of the zeta potential. These Zr-based nanoparticles are still
422 observed after P sorption (Figures S14c and d). The presence of Al hydroxides or boehmite rods in

addition to Zr0.1-A and Zr0.1-HT-P particles (Figures14) supported the results from ^{27}Al MAS NMR spectra, which show a significant AOH content (Table 3).

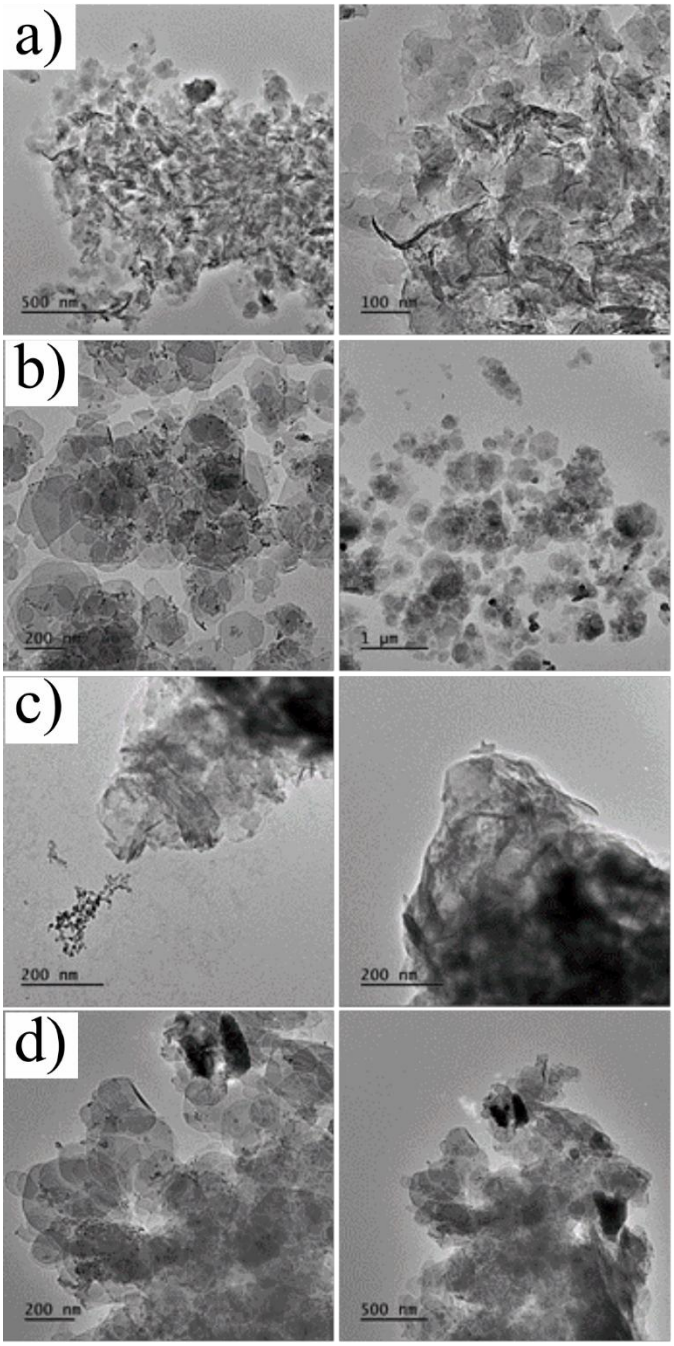

Figure 5. Two representative TEM images for each of a) Zr0.1-A, b) Zr0.1-HT), c) Zr0.1-A-P, and d) Zr0.1-HT-P.

Moreover, ^{25}Mg MAS NMR spectra supported a higher Mg:Al ratio in the LDH than the targeted 2:1 (Figure S15), in agreement with ^{27}Al-, ^{1}H MAS NMR, and ICP-OES, as the second order quadrupolar line shape is more undefined as the Mg:Al ratio increases (Sideris et al., 2012).

To summarize, Zr is segregated as amorphous $Zr(OH)_4$ for Zr0.1- and Zr0.5-A and as crystalline ZrO_2 for Zr0.1-HT and Zr0.5-HT, i.e., Zr is not incorporated into the LDH structure. The presence of ZrO_2 and $Zr(OH)_4$ is expected to influence the phosphate sorption capacity. Therefore, the theoretical sorption capacity can be estimated using the Mg:Al ratio from ^{27}Al MAS NMR and ICP-OES (Table S1) combined with the AOH and Zr(IV) content from ICP-OES. From the detailed characterization, it can be unambiguously concluded that the samples contain three phases: 1) MgAl-LDH 2) AOH, and 3) $Zr(OH)_4$ (aged samples) or ZrO_2 (hydrothermally treated). Based on ^{27}Al MAS NMR and ICP-OES the contribution from each phase can be calculated. The adjusted Mg:Al ratio in the MgAl-LDH and their removal capacities are summarized in Table S1. The LDH phase represents 90-98 mass% of the sample. The AOH and Zr (hydr)oxide content corresponds to 1-10 mass%, with $Zr(OH)_4/ZrO_2$ contribution 2-6 mol% based on ICP-OES. Thus, based on the Zr (hydr)oxide content, this phase accounts for less than 5 mgP/g (Table 1). Therefore, mainly the LDH and the AOH contribute to the sample's phosphate removal capacity. Finally, the decreased sorption capacity is a direct consequence of the decrease in Al content.

3.3.Characterization of the LDH after phosphate sorption

The phosphate loaded LDH (MgAl-A-P, MgAl-HT-P, Zr0.1-A-P, Zr0.1-HT-P, Zr0.5-A-P, and Zr0.5-HT-P) were characterized in detail to understand the stability of the LDH during P exposure and the pathway of removal.

As expected, phosphate sorption on the surface of aged and hydrothermally treated samples reversed the charge of the platelets. Thus, the zeta potential value changes from 29 - 27 mV (MgAl-A and MgAl-HT) to -17 mV (MgAl-A-P and MgAl-HT-P) (Table 3). No significant different is observed between the MgAl-LDH and the lowest Zr-doping level. Increasing the Zr(IV) content to 0.5 in the aged LDH leads to a clear change of surface charge from +29 mV to -12 mV. Hydrothermal treatment leads to phase segregation and formation of ZrO_2, which has limited effect on the mean (bulk) zeta potential (Table 3).

PXRD showed an increased stacking disorder and decrease in crystallinity of the phosphate loaded LDH (Table 3), also observed in the ^{1}H- and ^{25}Mg MAS NMR (Figures S10-11, S15), and in agreement with earlier studies of MgAl-LDH (Lundehøj et al., 2019a). The lower resolution of the ^{1}H MAS NMR spectra prevented unambiguous deconvolution and thereby determination of the Mg:Al ratio. However, ^{27}Al MAS NMR (Figure S16), FT-IR (Figure S5) and PXRD (Figure 1) supported preservation of the LDH structure, but with an increased stacking disorder. For example, the M-M distance in the LDH (unit cell parameter *a*) does not change after phosphate exposure (Table 3 and Figure S4). Similarly, ICP-OES (Table 1) and ^{27}Al MAS NMR shown no significant change in the bulk composition of Mg, Al, and Zr or relative concentration of the LDH, respectively.

The *c* unit cell parameters, i.e., the interlayer spacing, increases ca 0.5 Å after P sorption, which combined with the increase in the FWHM of the (00l) reflections (Table 3) reflects the intercalation of phosphate into the LDH as previously observed (Costantino et al., 1997; Hou et al., 2003; Lundehøj et al., 2019a). Moreover, the $\nu_3(PO_4^{3-})$ vibration (Badreddine et al., 1999) observed by FT-IR (Figure S5) also proves phosphate related to the material and the negative surface charge (-9 to -19 mV; Table 3) indicates surface complexation. To summarize, characterization show no changes in

the sample composition (i.e., limited dissolution and degradation) of the LDH layer after phosphate exposure but strong surface modifications.

3.4. Quantification of the different phosphate removal pathways by ^{31}P MAS NMR spectroscopy

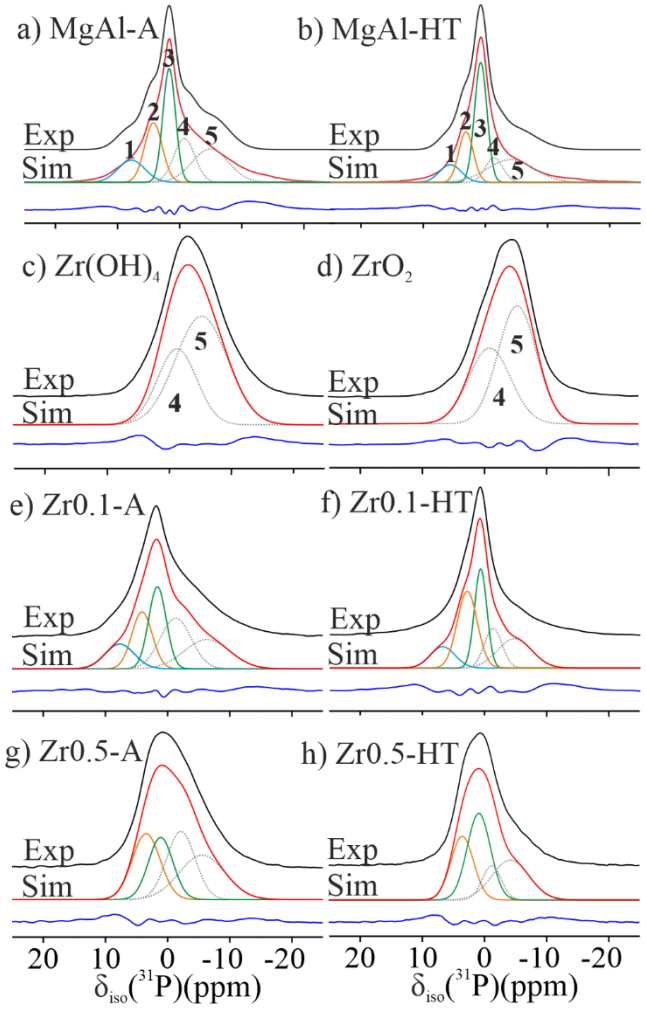

Figure 6. Experimental ^{31}P MAS NMR spectra of the LDH samples after phosphate sorption (a, b, e, f), $Zr(OH)_4$ (c), and ZrO_2 (d) and the respective deconvolutions with experimental (black), simulation (red), error (blue) and the individual sites: 1: turquoise, 2: orange, 3: green and site 4 and 5: grey.

To investigate the phosphate removal pathways and the different phosphate sites present, ^{31}P MAS NMR spectra were recorded (Figure 6). Deconvolution of the ^{31}P MAS NMR spectra of LDH can be challenging due to broad resonances and/ or overlapping sites as observed previously (Borges et al., 2019; Hou et al., 2003; Lundehøj et al., 2019a; Lundehøj et al., 2019b). Generally, each LDH here contains four or five different P sites, i.e., five different phosphorous local environments. These sites are ***site 1***: $\delta_{iso}(^{31}P)$ = 6.8 to 7.8 ppm, ***site 2*****:** $\delta_{iso}(^{31}P)$ = 2.9 to 4.2 ppm, ***site 3*****:** $\delta_{iso}(^{31}P)$ = 0.6-1.7 ppm, ***site 4*** $\delta_{iso}(^{31}P)$ = - 0.8 to -2.2 ppm and finally ***site 5*** $\delta_{iso}(^{31}P)$ = -4.1 to -6.4 ppm (details in Table S5)

Sites 2 (20 - 31%) and 3 (21 - 36%) account for most of the intensity and are therefore assigned to intercalation of ortho-phosphate in the LDH, given that it is the main removal pathway. This is agreement with phosphate related to a ZnAl-LDH were found at $\delta_{iso}(^{31}P)$ = 4.5(5) and 0.6(3) ppm doing phosphate sorption at pH 5 (Lundehøj et al., 2019b). Furthermore, two sites at $\delta_{iso}(^{31}P)$ = 3.2 ppm for HPO_4^{2-} and a site at 6.2 ppm for PO_4^{3-} were identified for MgAl-LDH based on visual inspection (Hou et al., 2003). These reported $\delta_{iso}(^{31}P)$ does not fully match the values for site 2 and site 3 (Table S5), but determination of the isotropic resonances in spectra with overlapping sites with overlapping resonances is less precise. Therefore, Sites 2 and 3 are assigned to intercalation of $H_xPO_4^{(3-x)-}$ species.

Sites 4 (10 - 26%) and site 5 (20 - 28%) are assigned to phosphate removed by AOH, and the Zr phase(s), $Zr(OH)_4$ for aged samples and ZrO_2 for hydrothermally treated samples, respectively. This was based on a comparison with ^{31}P MAS NMR spectra recorded for $Zr(OH)_4$-P and ZrO_2-P (Figure 6c and d) combined with previous studies (Lundehøj et al., 2019a; Lundehøj et al., 2019b). Differentiation between the AOH, $Zr(OH)_4$, and ZrO_2 cannot be done because of broad and overlapping resonances and is beyond the scope of this work.

Finally, Site 1 (4 - 12%; $\delta_{iso}(^{31}P)$ = 6.8 to 7.8 ppm) has the lowest intensity and is not detected for Zr0.5-A or Zr0.5-HT. Furthermore, this site is most prominent for aged samples, Therefore, this site is tentatively assigned to dissolution of the LDH, as the smaller particles are less stable. The lack of site 1 for Zr0.5-A and Zr0.5-HT is explained by the high Mg:Al ratio in the LDH.

Phosphate sorbed to impurities (AOH, $Zr(OH)_4$, and ZrO_2) is the major pathway (41 – 54%) for aged samples in accordance with ^{27}Al- and ^{1}H MAS NMR. For a comparison, the impurities contribute 34 – 38% for hydrothermally treated samples. Thus, the impurity content in the LDH must be controlled, otherwise the phosphate will be strongly bound to the impurities instead of readily released from the LDH. This will decrease the recyclability of the LDH sorbents.

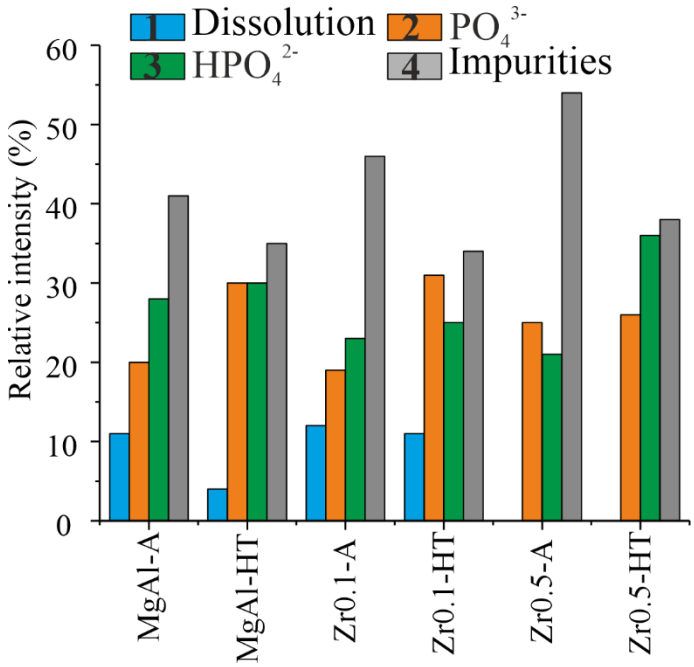

Figure 7. The relative intensity between the different ^{31}P sites and their assignment based on deconvolution of the ^{31}P MAS NMR spectra (Table S5). Dissolution and re-precipitation process

517 (blue), $H_xPO_4^{(3-x)-}$ removed by the LDH (orange and green) and the contribution from impurities, i.e.,
518 AOH, ZrO_2, $Zr(OH)_4$ (grey).
519
520 ## 4. Conclusions
521 Detailed insight into the phosphate removal capacity and stability of a series of MgAl-
522 LDH with different Zr(IV) modifications was achieved using global and local characterization
523 techniques. Our results clearly demonstrate, that Zr(IV) cannot be incorporated into the LDH lattice
524 and thereby improve the phosphate removal capacity. Instead separate phase of $Zr(OH)_4$ or ZrO_2 were
525 present for the aged and hydrothermal treated samples, respectively. Especially detection of the X-ray
526 amorphous $Zr(OH)_4$ in the aged samples required advanced characterization techniques (^{1}H- and ^{27}Al
527 MAS NMR, SEM, TEM and TGA). The unsuccessful incorporation of Zr(IV) together with the
528 decreased Al doping resulted in a drastic decrease in the phosphate removal capacity (45 - 54 to 16 - 20
529 mgP/g). Single pulse ^{31}P MAS NMR showed that 42 - 62% of the ortho-phosphate was intercalated in
530 the LDH by ion-exchange. However, ^{31}P MAS NMR also showed that up to 54% of phosphate was
531 removed by impurity phases or dissolution of the LDH. Thus, phosphate has a high affinity towards the
532 common impurities and the synthesis methods for LDH with limited impurities (coprecipitation
533 followed by hydrothermal treatment) is important for the reusability of the LDH based sorbents. Our
534 study clearly show that large particle size (crystallinity) is favored and that impurity phases should be
535 minimized. Moreover, it is emphasized that phosphate removal pathways cannot be reliably assessed
536 based on sorption studies only. Detailed characterization of the LDH sorbent before and after
537 phosphate exposure is paramount for reliable assessment of the LDH sorbent performance and stability.
538

Declaration of Competing Interest

The authors declare no competing interest.

Acknowledgments

The authors acknowledge The Danish Research Foundation (DFF Grøn Omstilling; grant: 95-305-23601-01130) and The Danish Research Council - Technology and Production Science (DFF–7017-00262) for financial support. The following people are thanked for their valuable help, discussions, and assistance with experimental data: lab. technicians Carina Lohman (ICP-OES) and Christian Brandt Jørgensen (SSNMR), Dr. Christian Henriksen (PXRD and Le Bail refinement), Dr Arkadiusz Jaroslaw Goszczak (SEM), Dr. Anders Bruhn Arndal Andersen (SSNMR) Mr. Lucas Urbano José (valuable discussions).

Appendix A. Supplementary data

Supporting information provide additional information about PXRD, Le Bail refinement, FT-IR, SEM, ^{1}H, ^{25}Mg, ^{31}P, ^{27}Al 1D MAS NMR together with 2D MAS NMR (^{27}Al 3QMAS) and kinetics experiments together with isotherm refinement parameters.

Data availability

Data will be available upon request.

References

Al Jaberi, M., Mallet, M., Greenwell, H.C., Abdelmoula, M., Ruby, C., 2019. Using Ca-Fe layered double hydroxide transformation to optimise phosphate removal from waste waters. Applied Clay Science 182, 105281.
Amoureux, J.P., Fernandez, C., 1998. Triple, quintuple and higher order multiple quantum MAS NMR of quadrupolar nuclei. Solid State Nuclear Magnetic Resonance 10, 211-223.
Arias, S., Sousa, L.V., Barbosa, C.B.M., Silva, A.O.S., Fréty, R., Pacheco, J.G.A., 2018. Preparation of NiAlZr-terephthalate LDHs with high Al and Zr content and their mixed oxides for cyclohexane dehydrogenation. Applied Clay Science 166, 137-145.
Ashekuzzaman, S.M., Jiang, J.-Q., 2014. Study on the sorption–desorption–regeneration performance of Ca-, Mg- and CaMg-based layered double hydroxides for removing phosphate from water. Chemical Engineering Journal 246, 97-105.
Badreddine, M., Legrouri, A., Barroug, A., De Roy, A., Besse, J.P., 1999. Ion exchange of different phosphate ions into the zinc-aluminum-chloride layered double hydroxide, Materials Letters.
Bekele, B., Lundehøj, L., Jensen, N.D., Nielsen, U.G., Forano, C., 2019. Sequestration of orthophosphate by $Ca_2Al\text{-}NO_3$ layered double hydroxide – Insight into reactivity and mechanism. Applied Clay Science 176, 49-57.
Bernardo, M.P., Guimarães, G.G.F., Majaron, V.F., Ribeiro, C., 2018. Controlled Release of Phosphate from Layered Double Hydroxide Structures: Dynamics in Soil and Application as Smart Fertilizer. ACS Sustainable Chemistry & Engineering 6, 5152-5161.
Borges, R., Wypych, F., Petit, E., Forano, C., Prevot, V., 2019. Potential Sustainable Slow-Release Fertilizers Obtained by Mechanochemical Activation of MgAl and MgFe Layered Double Hydroxides and K_2HPO_4. Nanomaterials 9, 183.
Bunce, J.T., Ndam, E., Ofiteru, I.D., Moore, A., Graham, D.W., 2018. A Review of Phosphorus Removal Technologies and Their Applicability to Small-Scale Domestic Wastewater Treatment Systems. Frontiers in Environmental Science 6.
Chitrakar, R., Tezuka, S., Hosokawa, J., Makita, Y., Sonoda, A., Ooi, K., Hirotsu, T., 2010. Uptake properties of phosphate on a novel Zr–modified MgFe–LDH(CO_3). Journal of Colloid and Interface Science 349, 314-320.
Chitrakar, R., Tezuka, S., Sonoda, A., Sakane, K., Ooi, K., Hirotsu, T., 2007. Synthesis and phosphate uptake behavior of Zr^{4+} incorporated MgAl-layered double hydroxides. Journal of Colloid and Interface Science 313, 53-63.
Cordell, D., Drangert, J.O., White, S., 2009. The story of phosphorus: Global food security and food for thought. Global Environmental Change 19, 292-305.
Cordell, D., White, S., 2014. Life's Bottleneck: Sustaining the World's Phosphorus for a Food Secure Future. Annual Review of Environment and Resources 39, 161-188.
Costantino, U., Casciola, M., Massinelli, L., Nocchetti, M., Vivani, R., 1997. Intercalation and grafting of hydrogen phosphates and phosphonates into synthetic hydrotalcites and a.c.-conductivity of the compounds thereby obtained. Solid State Ionics 97, 203-212.
Duan, X., Evans, D.G., 2005. Structural aspects of Layered Double Hydroxides. Springer.
Egle, L., Rechberger, H., Krampe, J., Zessner, M., 2016. Phosphorus recovery from municipal wastewater: An integrated comparative technological, environmental and economic assessment of P recovery technologies. The Science of the Total Environment 571, 522-542.
Everaert, M., Warrinnier, R., Baken, S., Gustafsson, J.-P., De Vos, D., Smolders, E., 2016. Phosphate-Exchanged Mg–Al Layered Double Hydroxides: A New Slow Release Phosphate Fertilizer. ACS Sustainable Chemistry & Engineering 4, 4280-4287.
Foo, K.Y., Hameed, B.H., 2010. Insights into the modeling of adsorption isotherm systems. Chemical Engineering Journal 156, 2-10.
Forano, C., Hibino, T., Leroux, F., Taviot-Gueho, C., 2006. Layered double hydroxides (LDH), in: Bergaya, F., Theng, B.K.G., Lagaly, G. (Eds.), Handbook of Clay Science. Elsevier, pp. 1021-1095.
Goh, K.-H., Lim, T.-T., Dong, Z., 2008. Application of layered double hydroxides for removal of oxyanions: A review. Water Research 42, 1343-1368.
Hall, R.L., Boisen Staal, L., Macintosh, K.A., McGrath, J.W., Bailey, J., Black, L., Gro Nielsen, U., Reitzel, K., Williams, P.N., 2020. Phosphorus speciation and fertiliser performance characteristics: A comparison of waste recovered struvites from global sources. Geoderma 362, 114096.
He, F., Zhuang, J., Lu, B., Liu, X., Zhang, J., Gu, F., Zhu, M., Xu, J., Zhong, Z., Xu, G., Su, F., 2021. Ni-based catalysts derived from Ni-Zr-Al ternary hydrotalcites show outstanding catalytic properties for low-temperature CO_2 methanation. Applied Catalysis. B: Environmental 293, 120218.
Hou, X., Bish, D.L., Wang, S.-L., Johnston, C.T., Kirkpatrick, R.J., 2003. Hydration, expansion, structure, and dynamics of layered double hydroxides. American Mineralogist 88, 167-179.
Imran, A., López-Rayo, S., Magid, J., Hansen, H.C.B., 2016. Dissolution kinetics of pyroaurite-type layered double hydroxide doped with Zn: Perspectives for pH controlled micronutrient release. Applied Clay Science 123, 56-63.

Intissar, M., Jumas, J.-C., Besse, J.-P., Leroux, F., 2003. Reinvestigation of the Layered Double Hydroxide Containing Tetravalent Cations: Unambiguous Response Provided by XAS and Mössbauer Spectroscopies. Chemistry of Materials 15, 4625-4632.
Jensen, N.D., Bjerring, M., Nielsen, U.G., 2016. A solid state NMR study of layered double hydroxides intercalated with para-amino salicylate, a tuberculosis drug. Solid State Nuclear Magnetic Resonance 78, 9-15.
Johir, M.A.H., Pradhan, M., Loganathan, P., Kandasamy, J., Vigneswaran, S., 2016. Phosphate adsorption from wastewater using zirconium (IV) hydroxide: Kinetics, thermodynamics and membrane filtration adsorption hybrid system studies. Journal of Environmental Management 167, 167-174.
Jupp, A.R., Beijer, S., Narain, G.C., Schipper, W., Slootweg, J.C., 2021. Phosphorus recovery and recycling-closing the loop. Chemical Society Reviews 50, 87-101.
Karthikeyan, J., Fjellvåg, H., Bundli, S., Sjåstad, A.O., 2021. Efficient exfoliation of layered double hydroxides; effect of cationic ratio, hydration state, anions and their orientations. Materials 14, 1-11.
Katz, G., 2006. X- Ray Diffraction Powder Pattern of Metastable Cubic ZrO_2. Journal of the American Ceramic Society 54, 531-531.
Kemp, T.F., Smith, M.E., 2009. QuadFit—A new cross-platform computer program for simulation of NMR line shapes from solids with distributions of interaction parameters. Solid State Nuclear Magnetic Resonance 35, 243-252.
Kim, T.H., Lundehøj, L., Nielsen, U.G., 2020. An investigation of the phosphate removal mechanism by MgFe layered double hydroxides. Applied Clay Science.
Koilraj, P., Kannan, S., 2010. Phosphate uptake behavior of ZnAlZr ternary layered double hydroxides through surface precipitation. Journal of Colloid and Interface Science 341, 289-297.
Lamastra, L., Suciu, N.A., Trevisan, M., 2018. Sewage sludge for sustainable agriculture: contaminants' contents and potential use as fertilizer. Chemical and Biological Technologies in Agriculture 5, 1-6.
Liu, Q., Wang, C., Qu, W., Wang, B., Tian, Z., Ma, H., Xu, R., 2014. The application of Zr incorporated Zn-Al dehydrated hydrotalcites as solid base in transesterification. Catalysis Today 234, 161-166.
Lombardo, G.M., Pappalardo, G.C., Punzo, F., Costantino, F., Costantino, U., Sisani, M., 2005. A Novel Integrated X-ray Powder Diffraction (XRPD) and Molecular Dynamics (MD) Approach for Modelling Mixed-Metal (Zn, Al) Layered Double Hydroxides (LDHs). WILEY-VCH Verlag, Weinheim, pp. 5026-5034.
Luengo, C.V., Volpe, M.A., Avena, M.J., 2017. High sorption of phosphate on Mg-Al layered double hydroxides: Kinetics and equilibrium. Journal of Environmental Chemical Engineering 5, 4656-4662.
Lundehøj, L., Cellier, J., Forano, C., Nielsen, U.G., 2019a. Atomic Level Understanding of Orthophosphate Adsorption by Magnesium Aluminum-Layered Double Hydroxides—A Multitechnique Study. The Journal of Physical Chemistry C 123, 24039-24050.
Lundehøj, L., Jensen, H.C., Wybrandt, L., Nielsen, U.G., Christensen, M.L., Quist-Jensen, C.A., 2019b. Layered double hydroxides for phosphorus recovery from acidified and non-acidified dewatered sludge. Water Research 153, 208-216.
Luo, X., Wu, X., Reng, Z., Min, X., Xiao, X., Luo, J., 2017. Enhancement of Phosphate Adsorption on Zirconium Hydroxide by Ammonium Modification. Industrial & Engineering Chemistry Research 56, 9419-9428.
Miyauchi, H., Yamamoto, T., Chitrakar, R., Makita, Y., Wang, Z., Kawai, J., Hirotsu, T., 2009. Phosphate Adsorption Site on Zirconium Ion Modified MgAl-layered Double Hydroxides. Topics in Catalysis 52, 714-723.
Motandi, M.K., Zhang, Z., Inkoua, S., Yan, L., 2022. Application of zirconium modified layered double hydroxide and calcination product for adsorptive removal of phosphate from aqueous solution. Environmental Progress & Sustainable Energy 41.
Nagul, E.A., McKelvie, I.D., Worsfold, P., Kolev, S.D., 2015. The molybdenum blue reaction for the determination of orthophosphate revisited: Opening the black box. Analytica Chimica Acta 890, 60-82.
Nielsen, U.G., 2021. Solid state NMR studies of layered double hydroxides, Annual Reports on NMR Spectroscopy. Elsevier, pp. 1-66.
Novillo, C., Guaya, D., Allen-Perkins Avendaño, A., Armijos, C., Cortina, J.L., Cota, I., 2014. Evaluation of phosphate removal capacity of Mg/Al layered double hydroxides from aqueous solutions. Fuel 138, 72-79.
Nowicki, J., Lach, J., Organek, M., Sabura, E., 2016. Transesterification of rapeseed oil to biodiesel over Zr-dopped MgAl hydrotalcites. Applied Catalysis A: General 524, 17-24.
Nuryadin, A., Imai, T., Kanno, A., Yamamoto, K., Sekine, M., Higuchi, T., 2021. Phosphate adsorption and desorption on two-stage synthesized amorphous-ZrO_2/Mg–Fe layered double hydroxide composite. Materials Chemistry and Physics 266, 124559.

Poonoosamy, J., Brandt, F., Stekiel, M., Kegler, P., Klinkenberg, M., Winkler, B., Vinograd, V., Bosbach, D., Deissmann, G., 2018. Zr-containing layered double hydroxides: Synthesis, characterization, and evaluation of thermodynamic properties. Applied Clay Science 151, 54-65.

Pushparaj, S.S.C., Forano, C., Prevot, V., Lipton, A.S., Rees, G.J., Hanna, J.V., Nielsen, U.G., 2015. How the Method of Synthesis Governs the Local and Global Structure of Zinc Aluminum Layered Double Hydroxides. The Journal of Physical Chemistry C 119, 27695-27707.

Pushparaj, S.S.C., Jensen, N.D., Forano, C., Rees, G.J., Prevot, V., Hanna, J.V., Ravnsbæk, D.B., Bjerring, M., Nielsen, U.G., 2016. Structural Investigation of Zn(II) Insertion in Bayerite, an Aluminum Hydroxide. Inorganic Chemistry 55, 9306-9315.

Rahman, M.M., Salleh, M.A.M., Rashid, U., Ahsan, A., Hossain, M.M., Ra, C.S., 2014. Production of slow release crystal fertilizer from wastewaters through struvite crystallization – A review. Arabian Journal of Chemistry 7, 139-155.

Reitzel, K., Bennett, W.W., Berger, N., Brownlie, W.J., Bruun, S., Christensen, M.L., Cordell, D., van Dijk, K., Egemose, S., Eigner, H., Glud, R.N., Grönfors, O., Hermann, L., Houot, S., Hupfer, M., Jacobs, B., Korving, L., Kjærgaard, C., Liimatainen, H., Van Loosdrecht, M.C.M., Macintosh, K.A., Magid, J., Maia, F., Martin-Ortega, J., McGrath, J., Meulepas, R., Murry, M., Neset, T.-S., Neumann, G.n., Nielsen, U.G., Nielsen, P.H., O'Flaherty, V., Qu, H., Santner, J., Seufert, V., Spears, B., Stringer, L.C., Stutter, M., Verburg, P.H., Wilfert, P., Williams, P.N., Metson, G.v.S., 2019. New Training to Meet the Global Phosphorus Challenge. Environmental Science & Technology 53, 8479-8481.

Rodríguez-Carvajal, J., 1993. Recent advances in magnetic structure determination by neutron powder diffraction. Physica. B: Condensed Matter 192, 55-69.

Shen, Y., Liu, D., Fan, L., Li, S., Gao, L., 2011. Simultaneous incorporation of palladium and zirconium ions in Mg–Al layered double hydroxides by co-precipitation. Applied Clay Science 54, 179-183.

Sideris, P.J., Blanc, F.d.r., Gan, Z., Grey, C.P., Brookhaven National, L., 2012. Identification of Cation Clustering in Mg–Al Layered Double Hydroxides Using Multinuclear Solid State Nuclear Magnetic Resonance Spectroscopy. Chemistry of Materials 24, 2449-2461.

Staal, L.B., Charan Pushparaj, S.S., Forano, C., Prevot, V., Ravnsbæk, D.B., Bjerring, M., Nielsen, U.G., 2017. Competitive reactions during synthesis of zinc aluminum layered double hydroxides by thermal hydrolysis of urea. Journal of Materials Chemistry A 5, 21795-21806.

Talboys, P.J., Heppell, J., Roose, T., Healey, J.R., Jones, D.L., Withers, P.J.A., 2016. Struvite: a slow-release fertiliser for sustainable phosphorus management? Plant and Soil 401, 109-123.

van Meerten, S.G.J., Franssen, W.M.J., Kentgens, A.P.M., 2019. ssNake: A cross-platform open-source NMR data processing and fitting application. Journal of Magnetic Resonance 301, 56-66.

Velu, S., Sabde, D.P., Shah, N., Sivasanker, S., 1998. New Hydrotalcite-like Anionic Clays Containing Zr^{4+} in the Layers: Synthesis and Physicochemical Properties. Chemistry of Materials 10, 3451-3458.

Walan, P., Davidsson, S., Johansson, S., Höök, M., 2014. Phosphate rock production and depletion: Regional disaggregated modeling and global implications. Resources, Conservation and Recycling 93, 178-187.

Wang, D., Zhang, X., Cong, X., Liu, S., Zhou, D., 2018. Influence of Zr on the performance of Mg-Al catalysts via hydrotalcite-like precursors for the synthesis of glycerol carbonate from urea and glycerol. Applied Catalysis A: General 555, 36-46.

Wang, H., Yang, Z., Zhan, X., Wu, Y., Li, M., 2017. NiAlZrW hydrodesulfurization catalysts derived from tungstate intercalated NiAlZr layered double hydroxides. Fuel Processing Technology 160, 178-184.

Wilfert, P., Kumar, P.S., Korving, L., Witkamp, G.-J., van Loosdrecht, M.C.M., 2015. The Relevance of Phosphorus and Iron Chemistry to the Recovery of Phosphorus from Wastewater: A Review. Environmental Science & Technology 49, 9400-9414.

Wu, B., Wan, J., Zhang, Y., Pan, B., Lo, I.M.C., 2020. Selective Phosphate Removal from Water and Wastewater using Sorption: Process Fundamentals and Removal Mechanisms. Environmental Science & Technology 54, 50-66.